Applied Ocean Research 101 (2020) 102225

Contents lists available at ScienceDirect

Applied Ocean Research

journal homepage: www.elsevier.com/locate/apor

Sensitivity analysis of friction and creep deformation effects on preload relaxation in offshore wind turbine bolted connections

Jarryd Braithwaite, Iñigo Gómez Goenaga, Behrooz Tafazzolimoghaddam, Ali Mehmanparast*

Offshore Renewable Energy Engineering Centre, Cranfield University, Cranfield MK43 0AL, UK

ARTICLE INFO

Keywords:
Offshore wind turbine
Foundation to transition piece connection
Short-term relaxation
Creep power law
Ramberg-Osgood

ABSTRACT

A considerable portion of the preload loss in offshore wind turbine foundation to transition piece flanged connections is caused by short-term relaxation of the bolts. This relaxation can be influenced by several factors including the friction coefficient between the contact pairs in the flange bolted connections as well as room temperature creep. The present study focuses on the effect of these two factors on the performance of M72 bolts in offshore wind turbines. A detailed finite element model of a one-bolt-segment of the flanged connection is developed with material properties obtained from the literature. The first analysis examines the response of the bolt to a change in friction coefficient between contact surfaces. In the second analysis, the effect of room temperature creep is investigated over the first 48 hours of operation. Although creep is usually neglected in such low temperatures, for high load levels close to the material's yield stress, significant creep strain rates can occur. Finally, a sensitivity analysis on both friction and creep properties is carried out to investigate the influence of these two factors on the preload relaxation of M72 bolted connections.

1. Introduction

Monopile foundations are currently the most popular support structures, accounting for over 80% of the offshore wind installations in Europe [1,26–28,30]. The wind turbine tower is usually mounted onto to the monopile substructures via a transition piece, which is designed to absorb tolerances and inclinations of the system. The transition piece is fixed to the substructure by either grouting or using a bolted flange connection. Grouted connections are widely used with offshore wind monopiles and are conventionally covered by standards. There have however been several incidents where these connections failed to perform sufficiently and showed signs of failure leading to high operation and maintenance (O&M) costs [2–4].

Recently, the industry has shown more interest in bolted flange connections due to the issues with grouted connections, as well as advantages of bolted connections which can lead to a faster and more cost effective installation [29]. Flanged connections are widely used in the oil and gas industry, as well as for onshore wind turbines, however at a much reduced scale in both cases. M72 and M64 bolts are the most popular fasteners used in the offshore wind industry [5]. Despite the difficulty caused by the enormous dimensions and weight of these bolts, these are of great importance for performance of the connections. There are four scaling factors affecting bolts; geometric, technological, statistical and surface technological [6]. The last three are relevant only when performing experiments, which is not the immediate aim of the present study. However, the geometrical size effect should be taken into account for the finite element analysis (FEA) modelling as the stress gradient from the threaded surface (with high stress) toward the centre of the bolt decreases when the diameter of the bolt increases [7].

There are still some concerns surrounding bolted flange connections due to issues such as bolt interaction and tightening sequence [8], or pre-tensioning and relaxation effects, which can cause an increase in maintenance costs. Considering that the O&M costs in offshore wind industry constitute up to 35 % of the total cost, reducing or eliminating one possible failure mode might result in a significant reduction in the levelised cost of energy (LCOE) [9,24,25]. In order to achieve the aforementioned LCOE, it is estimated that a 3 to 10% cost reduction is expected to be achieved from substructure, cabling and substation costs alone [10].

Preload relaxation is one of the key factors in bolted flange

Abbreviations: O&M, operation and maintenance; RO, Ramberg-Osgood; RT, room temperature; LT, low temperature; EXT, external contact; TT, thread to thread contact; FF, flange to flange contact; LCOE, levelised cost of energy; σ_y, yield stress; T_F, melting temperature; ε, strain; E, elastic Young's modulus; σ, applied stress; α, yield offset; K, RO material constant; N, RO material constant; UTS, ultimate tensile strength; $\dot{\varepsilon}_{cr}$, average creep strain rate; A, creep power-law multiplier; n, power-law creep index; μ, friction coefficient; μ_{TT}, friction coefficient for thread to thread contact; μ_{EXT}, friction coefficient for external contact

* Corresponding author.
E-mail address: a.mehmanparast@cranfield.ac.uk (A. Mehmanparast).

https://doi.org/10.1016/j.apor.2020.102225
Received 7 August 2019; Received in revised form 23 April 2020; Accepted 25 May 2020
Available online 08 June 2020

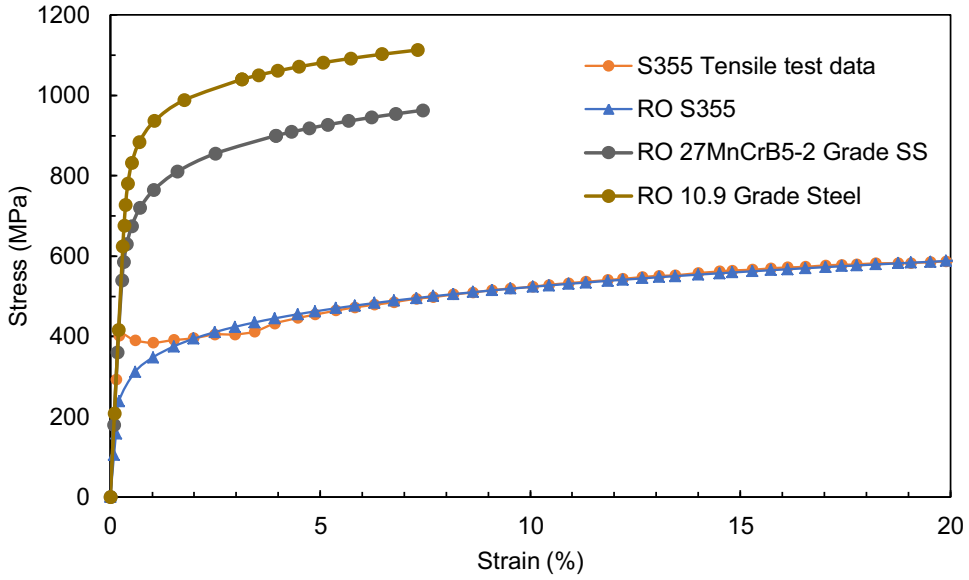

Fig. 1. Stress-strain curves for the materials employed in the present study.

connections that can lead to a loss of clamping forces in the flanged connection. Relaxation of the bolts can cause a reduction in preload and consequently, a loss of clamping force in the flange. This can either be the result of long term effects, such as cyclic loading, or the result of short-term effects happening during or immediately after preload application. In the present work, only short-term relaxation is considered. According to Kulak et al [11], short-term relaxation can cause a loss of preload up to 11% in the first hours of tightening.

Short-term relaxation can be the result of early plastic deformation in some regions of the bolt, particularly in the thread or below the head of the bolt. It is known that all flange connection surfaces have some degree of imperfection as a result of the fabrication or production process. Because of these imperfections, the surfaces will not be in full contact and the load is not evenly distributed, resulting in regions with stresses higher than the yield stress, σ_y. The contact points with higher stress will deform plastically and will cause the surfaces to gradually level out, increasing the contact area and eventually eliminating the high stress areas. This plastic deformation process is called embedment.

Creep is usually described as a time dependent deformation under fixed stress and at elevated temperatures, which are usually over 0.5 times the melting temperature, T_F, of the material [12]. Although these conditions are not applicable to wind turbines, it has been found that creep at lower temperatures is still possible. The magnitude of low temperature creep is obviously smaller than a high temperature case, which is why it is usually neglected. For a high strength steel similar to that of M72 bolts, even at stresses as low as a third of σ_Y, some creep deformation exists. Also, Liu et al. [13] reported that higher creep deformation is expected in high strength steel (with σ_Y of 1250 MPa) for stresses close to the yield stress. In the present study, preload stresses of 0.9 σ_Y are considered.

The relaxation begins to occur immediately after installation due to a range of short-term effects, including frictional effects and low temperature creep. There are other factors that lead to short-term relaxation, although with smaller influence, such as thread engagement, misalignment [22] between bolt and hole, improper bolt-hole dimensioning [14] or residual stresses in the structure itself [15], none of which are considered in the present paper. In this paper, the short term preload relaxation is analysed based on the effects of friction and low temperature creep using FEA modelling in Abaqus software based on a representative flange section connected using M72 bolts. The effect of variation in friction on the preload loss is studied for different sets of contact surfaces in order to describe the desirable friction coefficient (i.e. surface quality) for each part. For the creep effect, short-term response of the bolt is compared for three different materials with different yield stresses in order to find out the significance of the effect of creep deformation on preload relaxation. The purpose of this study is not to exactly predict the preload loss due to creep deformation, but instead to determine if its effect on relaxation is considerable by performing a set of sensitivity analyses.

2. Material models

Three different materials were considered for the current study:

- S355 structural steel for the flange (EN10025 standard)
- 27MnCrB5-2 grade stainless steel for the washer (EN 1.7182 standard)
- 10.9 grade high strength steel for the bolt and nut (ASTEM A325 standard)

A tensile test was performed on S355 steel to enable a detailed analysis and verification of a simplified Ramberg-Osgood (RO) material model. Subsequently, the tensile behaviour of the other two materials examined in this study, for which the tensile data are not readily available in the literature, was generated using the basic mechanical properties of these two materials.

2.1. Ramberg-Osgood material model

Abaqus software allows employment of a modified version of the Ramberg-Osgood material model to describe the elastic and plastic behaviour of the material based on the following relationship [16]:

$$\varepsilon = \frac{\sigma}{E} + \alpha\frac{\sigma}{E}\left(\frac{\sigma}{\sigma_Y}\right)^N \tag{1}$$

where ε is the strain, E is the elastic Young's modulus, σ is applied stress, α is the yield offset, and K and N are material constants. Where limited tensile data are available for a given material, the tensile curve can be generated by employing the RO material model and using the values of yield (usually according to the 0.2 % criteria) and ultimate tensile strength (UTS) of the tensile curve. The material constants in the RO model can be found by fitting a curve that passes through these two points and the origin. To validate the accuracy of the model, an analysis of the tensile test data for S355 steel was carried out. Fig. 1 shows the

Table 1
Ramberg-Osgood material model.

	σ_Y (MPa)	UTS (MPa)	Strain corresponding to UTS (%)	α	N
S355	356	537	19.89	2.17	9.7
27MnCrB5-2	754	1026	13.10	1.55	10.1
10.9 grade steel	946	1134	8.62	1.43	14.0

stress-strain curves for all three materials, calculated from the RO model. Tensile test data was available for S355 and hence this data can be used directly in Abaqus to define the material properties. However, no test data was available for the additional two materials and therefore the data from the RO material model was used in Abaqus to define their elastic-plastic properties. The graph shows that the S355 curve determined using the RO model agrees well with the tensile test data and therefore it is determined that the model is suitable for all materials.

Once the simplified RO model was validated using the S355 tensile data, the material dependent constants were identified which are summarised in Table 1. Also included in this table are the RO material dependent constants for the washer and bolt materials.

2.2. Elastic-plastic-creep model

In order to simplify the analysis in the present study, the elastic-plastic-creep behaviour is only assumed for the bolt and nut with stresses close to σ_Y. While the elastic-plastic material response is predicted based on a uniform set of points using the RO model for the bolt material (i.e. 10.9 grade steel), the following power law equation is used to describe the average creep strain rate of the material [17]:

$$\dot{\varepsilon}_{cr} = A\sigma^n \tag{2}$$

where A and n are material and temperature dependent constants. This model is implemented in Abaqus using the time hardening creep property to describe the average creep strain rate which accounts for the primary, secondary and tertiary creep region. There is no data available in the literature for 10.9 grade steel creep properties at room temperature, therefore the material data by Alfredsson et al. [18] is used which provides two sets of properties for bainite and martensite high strength steels at a relatively low temperature of 75°C. While bainite has a higher σ_Y than 10.9 grade steel (around 1600 MPa according to [18]), the martensite has a lower σ_Y than that the bolt material (760 MPa).

Creep is a time-independent deformation mechanism and the power-law is developed by taking the initial value of creep strain rate at different stresses. These values were fitted into the creep equation in a procedure similar to that used for Ramberg-Osgood constants. Both sets of constants for the materials have either higher (bainite) or lower (martensite) σ_Y than the bolt material and therefore an intermediate material model is created to represent a material with average properties between the two. The n constant is obtained by an arithmetic average of the corresponding values for the other two materials. For A, given the nature of the formula, geometrical averaging is used. The power-law creep model constants employed in this study can be seen in Table 2.

Table 2
Three sets of power-law creep constants.

	A [h^{-1} MPa^{-n}]	n
Bainite	3.532×10^{-30}	8.75
Martensite	1.820×10^{-16}	4.80
Combined	$2.536E \times 10^{-23}$	6.77

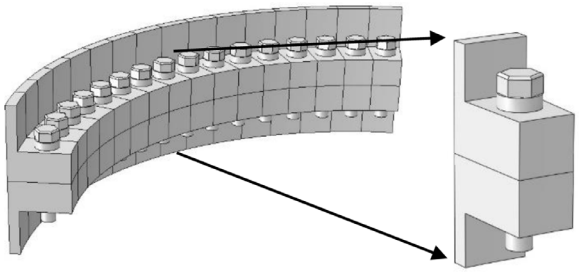

Fig. 2. The flange segment design in Abaqus.

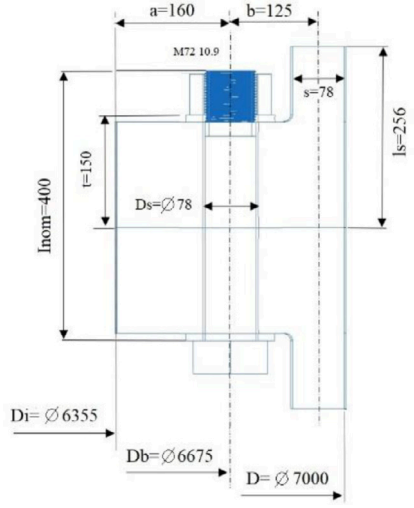

Fig. 3. Flange dimensions.

3. Finite element model set-up

A flange segment, representative of a 160-bolt flange configuration, was modelled in Abaqus. This included the bolt, nut, washers and the upper (i.e. for transition piece) and lower (for monopile) flange sections, as depicted in Fig. 2. The dimensions of the original flange, which were taken from [5], are shown in Fig. 3. Note that small details such as the radius between flange and the wall are neglected, as well as the angled gap between the flanges. The bolt, nut and washers are designed according to ISO4032 standards for M72 bolts [19]. A 4 mm pitch M72 bolt was modelled, considering the minimum values within the tolerances.

3.1. Loading and boundary conditions

For short-term relaxation, both preload and gravitational loads were applied. External cyclic and long term loads are only considered for long-term relaxation studies and were therefore not considered in the present study. The bolt load is taken as 2914 kN for the M72 bolt, which results in stresses close to 90% of the material's yield stress, often known as the maximum safety limit for bolt tightening in the offshore wind industry. To apply the bolt preload, the 'Bolt load' command in Abaqus was used. In this approach, the focus is on the middle section of the bolt from which a portion of the bolt's length is subtracted. This amount of shortening depends on the value of preload that is expected. With this reduced bolt length, while keeping the rest of the assembly unchanged, the same load state as in real bolted connections is achieved. To allow short-term creep deformation to be considered in the analysis in the following steps, the 'Fix at current length' option for the bolt load was selected. This option allows the bolt to behave naturally and relax due to the creep effects.

Two boundary conditions were defined for the flange connection.

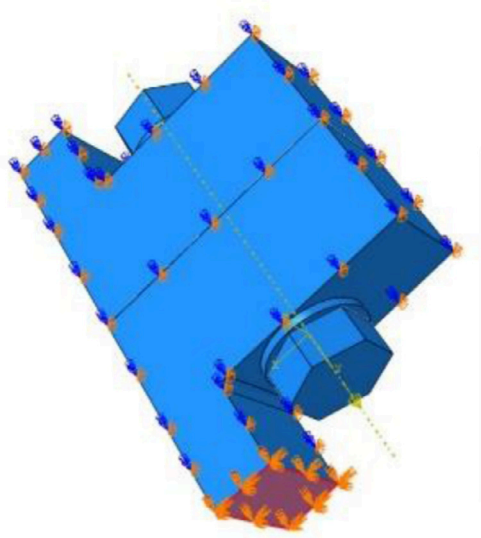

Fig. 4. Boundary conditions.

'Encastre' boundary condition was applied on the top surface, as shown in Fig. 4, to consider the wind turbine structure. The second boundary condition was used to limit lateral movement in the flange, as this modelled geometry is a segment of a larger structure with each segments movement restricted by the neighbouring segments. Symmetric boundary condition was used for the side surfaces (Fig. 4).

3.2. Contact definition

Contact surfaces were divided into three groups; flange to flange contact (FF contact), thread to thread contact (TT contact) and external contacts (EXT contact) such as the contact between washers, bolt, nut and flange. A friction coefficient was assigned to each contact using the 'Friction: Penalty' option in Abaqus. The FF contact properties remained constant throughout all of the simulations with a friction coefficient of $\mu = 0.84$. On the other hand, the μ values for TT (μ_{TT}) and the EXT (μ_{EXT}) contacts varied depending on a range friction scenarios. The friction coefficients, μ, examined in the simulations were selected from the values of 0.14, 0.25, 0.5 and 0.84.

3.3. Mesh definition

Tetrahedral elements were used to mesh all of the elements due to their simplicity for meshing complex geometries (see Fig. 5). The washer was the only exception which was meshed by hexahedral elements. Due to the shape of the threads in the nut and bolt geometries, special care was taken for the mesh generation. Several partitions were created to limit the total number of elements, however, a large number of elements were needed for such a complicated model. The mesh verification analysis revealed only 0.05 % of bolt and nut elements with aspect ratios higher than 10 and angular limits below 0.1% which is well within the acceptable range [20].

4. Analysis of friction effects on preload distribution

A sensitivity analysis of the friction coefficient effects on the response of the bolted connection is performed for a range of μ values, from steel-to-steel contact ($\mu_{TT} = 0.84$) to an average lubricated surface ($\mu_{TT} = 0.14$) [23]. In this study, the effects of thread friction and head/nut friction are analysed independently.

4.1. Thread friction analysis

For the thread friction analysis, four different μ values in the thread (TT contact) were considered whilst keeping the contact properties in the remaining surfaces (EXT contact) unchanged. This analysis was carried out to determine the extent that the TT friction affects the overall behaviour of the bolt and the mechanisms involved. Also, two different EXT contact friction values were studied to further analyse the influencing factors.

The first set of simulations were carried out for $\mu_{EXT} = 0.84$. Fig.6 shows the von-Misses stress distribution under two different TT friction conditions. For the measurements, the threads are assigned a number from 1 to 15, starting from the first engaged thread at the washer-nut contact (Fig. 6). The figure shows that the stresses at the centre of the bolt are slightly higher when the threads have a lower friction coefficient.

Making an in-depth analysis of the stresses for each thread, several points in each of the threads have been selected on both the roots and crests of the threads. From these points, the average and maximum stress values for each thread have been calculated, from thread 1 to 15. The Table 3 summarises the maximum stress values achieved for different values of TT friction coefficient and the maximum values at individual threads are shown in Fig. 7. The results show that as the TT friction coefficient increases, higher local values of stress in the contact points are measured. Assuming that plastic deformation is related to the maximum local stresses, using lubricated contacts can reduce this risk by lowering the stress by up to 3.5%.

From the results shown in Fig. 7, it appears that the first five threads show higher values of stress, indicating that these threads have a higher engagement and therefore are bearing a high percentage of the preload. From thread 6 onwards the stress levels gradually reduce towards the final thread, with the largest reduction in stress being observed at thread number 10. From the thread-by-thread analysis, it can be seen that the engagement level at every thread changes with friction. It can also be observed that a higher μ results in a higher stress in the first few threads, hence increasing the chance of plastic deformation. However,

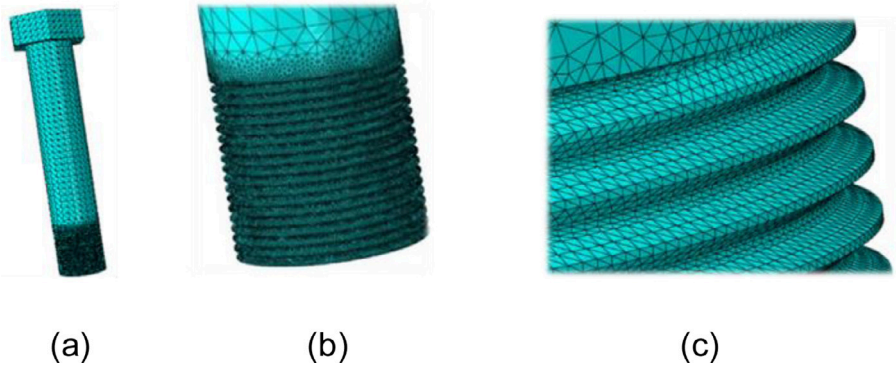

Fig. 5. Detail of the mesh in the thread regions (a) bolt, (b) threaded section of the bolt, (c) mesh details in the threaded section.

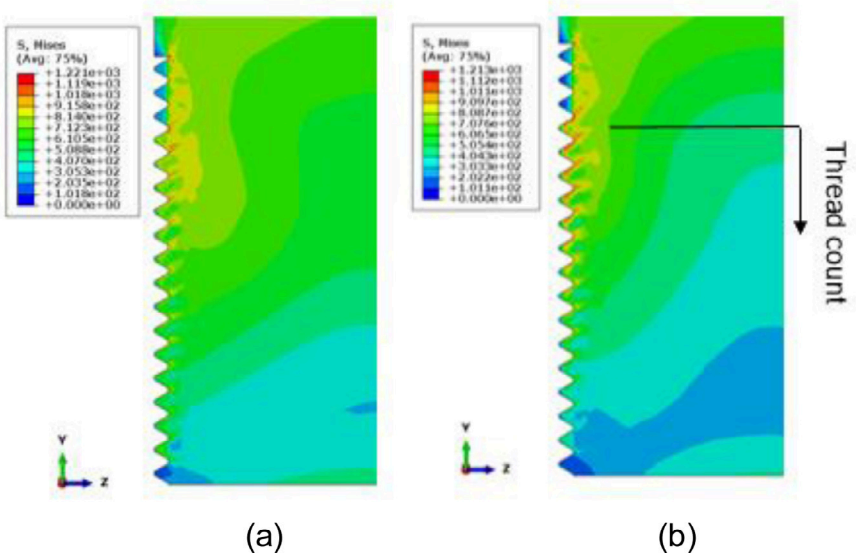

Fig. 6. von-Mises stress distribution in the bolt cross section for, (a) $\mu_{TT}=0.14$, and (b) $\mu_{TT}=0.84$. The external friction $\mu_{EXT}=0.84$ in both cases.

Table 3
Maximum stress at each group of threads (for μ_{EXT} 0.84). All stress values are in MPa.

μ_{TT}	0.14	0.25	0.5	0.84
Stress in threads 1 – 3	1098	1109	1130	1136
Stress in threads 4 – 6	1008	1025	1062	1073
Stress in threads 7 – 9	885	916	968	975
Stress in threads 10 – 12	713	746	740	730
Stress in threads 13 – 15	557	487	396	381

Table 4
Maximum stress at each group of threads (for μ_{EXT} 0.14). All stress values are in MPa.

μ_{TT}	0.14	0.25	0.5	0.84
Stress in threads 1 – 3	1059	1063	1077	1113
Stress in threads 4 – 6	1027	1034	1056	1093
Stress in threads 7 – 9	959	971	1001	1000
Stress in threads 10 – 12	917	926	913	852
Stress in threads 13 – 15	834	742	588	512

the stresses fall sharply towards the final threads, therefore reducing the risk of plastic deformation. From these results it is apparent that a low friction coefficient in the threads improves the distribution of the mechanical bolt load.

The same set of simulations was repeated considering $\mu_{EXT}=0.14$ and the results are shown in Table 4 and Fig. 8. The analysis of maximum thread stress in Table 4 shows a similar trend to Table 3. Interestingly, the values show that a reduction in EXT friction results in lower maximum stress levels. The differences between the stress values at TT 0.14 and 0.84 are also shown to be larger when compared to the results for $\mu_{EXT}=0.84$. Comparing the results from Tables 3 and 4, maximum thread stress is reduced by 7 % in the first threads when both μ_{TT} and $\mu_{EXT}=0.14$, compared to the maximum value in Table 3. However, when comparing the last threads in the bolt the stress value more than doubles for the same friction coefficients.

Fig. 8 shows a similar trend as Fig. 7, however the difference in TT friction coefficient is now much more pronounced. The difference between the curves across the first ten threads is still relatively small, however after this point it is clear that a lower TT friction coefficient results in a much higher level of stress in the final threads.

The average stress across all of the threads is calculated and presented in Table 5 for each of the friction scenarios in this section. The results show that reducing the value of μ_{TT} friction has a negligible effect when μ_{EXT} is 0.84. However, when EXT friction is reduced to 0.14 there is an improvement in average stress for all values of μ_{TT}, with the highest level of stress when both μ_{TT} and μ_{EXT} are 0.14, an increase of around 15%. Note that having higher stresses in the final threads (toward the end of the bolt) is an indicator of a more efficient bolt and nut

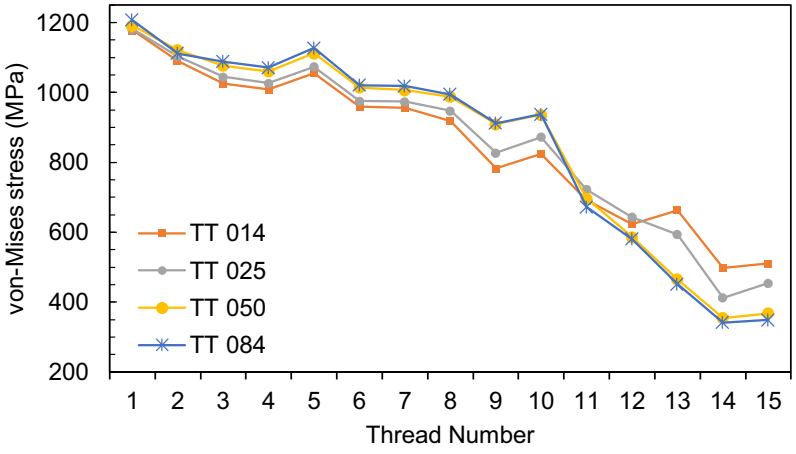

Fig. 7. Maximum stresses per thread (for μ_{EXT} 0.84).

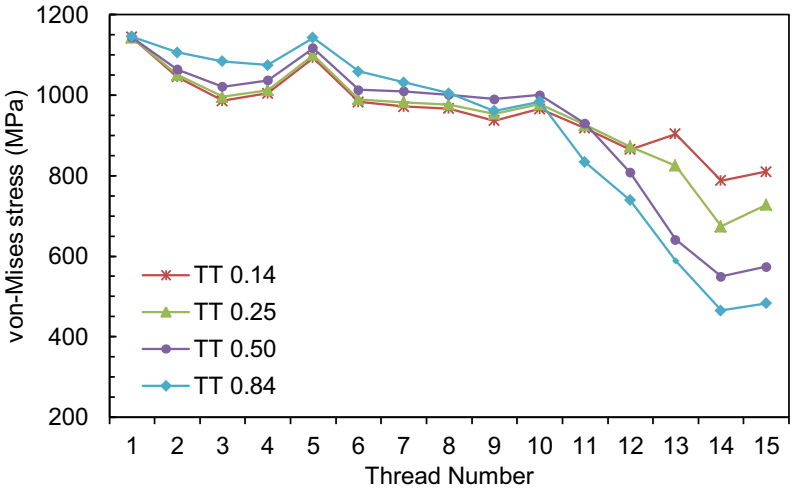

Fig. 8. Maximum stresses per thread (for μ_{EXT} 0.14).

Table 5
Average von-Mises stress in the thread (TT analysis).

μ_{TT}	0.14	0.25	0.5	0.84
μ_{EXT} = 0.84	630	626	623	624
μ_{EXT} = 0.14	724	712	690	674
Difference (%)	14.9%	13.7%	10.7%	8%

Table 6
Analysis of contact pressure between flanges (TT analysis).

μ_{TT}	0.14	0.25	0.5	0.84
μ_{EXT} = 0.84	107	108	108	108
μ_{EXT} = 0.14	113	113	113	113
Difference (%)	5.6%	4.6%	4.6%	4.6%

connection with a more even distribution of the load, as well as reducing the risk of plasticity. Finally, evaluating the contact pressure in all scenarios, the results in Table 6 show that thread friction has a negligible effect on the contact pressure between flanges, however there is an improvement of around 5% when the value of EXT friction is reduced.

4.2. External friction analysis

For the general friction simulations, the friction coefficient in TT contacts remains constant whilst varying μ_{EXT} for the values 0.14, 0.25, 0.5 and 0.84. Two different TT friction conditions were also used to check the consistency of the results. Fig. 9 shows a similar trend to Section 4.1, where a higher friction coefficient leads to higher stresses at the first threads and gradually reducing toward the final threads. From the graphs in Figs. 10 and 11, for both high and low TT friction coefficients, the effect of variation in μ_{EXT} is reversed at the fourth thread. Higher μ results in lower stress in the first three threads, however the effect is reversed after this point. Although the stress distribution has improved, it is not certain that a low friction coefficients for EXT contacts will reduce global plasticity.

Fig. 10 shows the difference in EXT friction coefficient is now much more pronounced. The difference between the curves across the first ten threads is still relatively small, however after this point it is clear that a lower EXT friction coefficient results in a much higher level of stress in the final threads. Reducing EXT friction also affects the average stress of the thread similar to TT friction reduction, as shown in Table 7. The average stress increases 8 % with lubricated EXT contacts when the TT contact μ is 0.84. For TT when the μ value is reduced to 0.14, the difference reaches 15 %. It has to be noted that when analysing the effect of changing the TT friction, the maximum increment reached is only 8%. Therefore, it is concluded that the EXT contacts friction coefficient is more determinant for the average stress state.

Comparing the results in Table 8, it can be seen that the contact pressure is independent of the friction coefficients of the thread. However, there can be a difference of up to 5% in the contact pressure between the flanges with EXT contacts properly lubricated to give a low friction coefficient.

5. Analysis of low temperature creep effects on preload distribution

In this section the effects of low temperature creep on the preload distribution in bolted connection is analysed. The aim is to demonstrate the influence of creep at low temperatures in a 48 hour period. For this analysis the applied load level and friction coefficients are kept constant to evaluate the influence of creep properties on preload distribution in M72 bolted connections.

5.1. Comparison of creep properties effects on preload

Different creep properties were simulated for materials with lower and higher yield strengths than that of 10.9 grade steel. These simulations are repeated with a third set of creep properties deduced by averaging the creep constants with the procedure described in Section 2.2. The three models are created for conditions of 75°C, as the lowest temperature creep properties found in the literature, and the assumption that the initial (and maximum) strain rate of the material applies for a 48-hour period. This is an overestimation, however, the main purpose of this study is not finding the exact value of creep but to examine whether or not preload relaxation is sensitive to time-dependent creep deformation through a comprehensive sensitivity analysis.

In order to evaluate the creep effects, the evolution of the average stress at the midsection of the bolt shaft has been measured. Fig. 12 shows the effect of power-law creep on the stress distribution in a bolted connection during 48 hours. Table 9 shows the total relaxation after a 48-hour period. It is evident in Fig. 12 and Table 9 that the creep deformation reduces the preload, and consequently, the clamping force of the flange. Clearly, softer materials (martensite) experience higher relaxations due to a greater extent of time-dependent elongation of the bolt as a result of creep deformation. This is caused by the relation between bolt's length and preload in elastic-plastic-creep analysis. Initially, creep rate and stress are expected to be constant at each point with a straight creep strain curve. However, the bolt's length has increased because of creep strain, which reduces the clamping force or in

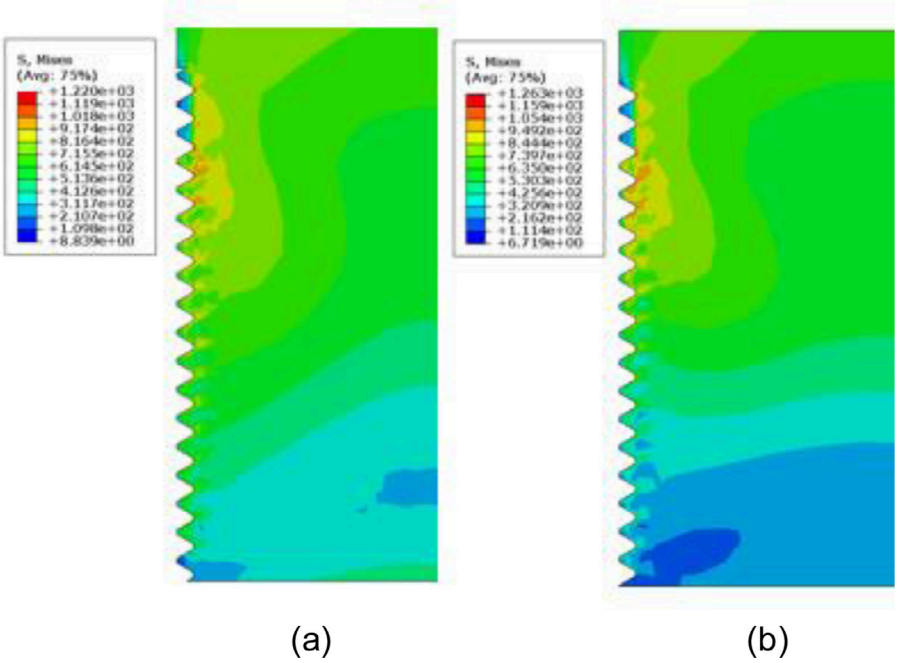

Fig. 9. von-Mises stress distribution in the bolt cross section for, (a) $\mu_{EXT} = 0.14$, and (b) $\mu_{EXT} = 0.84$. The external friction $\mu_{TT} = 0.14$ in both cases.

other words, the bolt is relaxing. As a consequence, $\dot{\varepsilon}_{cr}$ reduces over time, even when time hardening (m parameter in Eq. (2)) is not considered.

5.2. Creep sensitivity analysis

According to Mehmanparast et al. [21,31], the power index, n, in the creep law is not affected by temperature changes and can be assumed constant for a wide range of temperatures, while the power law multiplier A can be described as a function of temperature in most steels. In their work they have demonstrated that n stays almost unchanged when temperature changes, however, the value of A decreases continuously with temperature.

Since the lowest temperature creep properties found in the literature are at 75°C, an attempt has been made to estimate the lower temperature (i.e. at room temperature) creep properties following the approach given in [21]. For the present study n is kept unchanged (i.e. same as 75°C as suggested in [21]) and the sensitivity analysis over the creep multiplier constant, A, is performed. Three materials are studied, comparing the initial properties with A reduced by factors of 2 and 5, and the results are shown in Fig. 13. This final value has been set as an idealized assumption, considering that this rate of change over every 50 degrees at higher temperatures is respected for the present conditions, and therefore representing creep properties at 20 °C (i.e. room temperature). As mentioned earlier, the purpose of this study is not to precisely quantify creep properties at room temperature conditions, but to see the possible magnitude, and influence of power law reigning parameters.

In Fig. 13 bolt load during a 48-hour period is depicted for the three materials for A, $A/2$ and $A/5$. As expected, lower values of A reduce the $\dot{\varepsilon}_{cr}$ and therefore the amount of bolt relaxation. However, when the value of power law multiplier is halved, this does not result in the same proportion of reduction in preload. In Tables 10–12 the variation of preload loss after the 48-hour period is listed. It is interesting to see that even for bainite (the hardest material) there is still a 6% reduction of stress when A is reduced by a factor of 5. Comparison of Tables 10–12 shows that martensite is the most sensitive to a changes in A with remarkably larger relaxation. Hence, selecting a harder material with

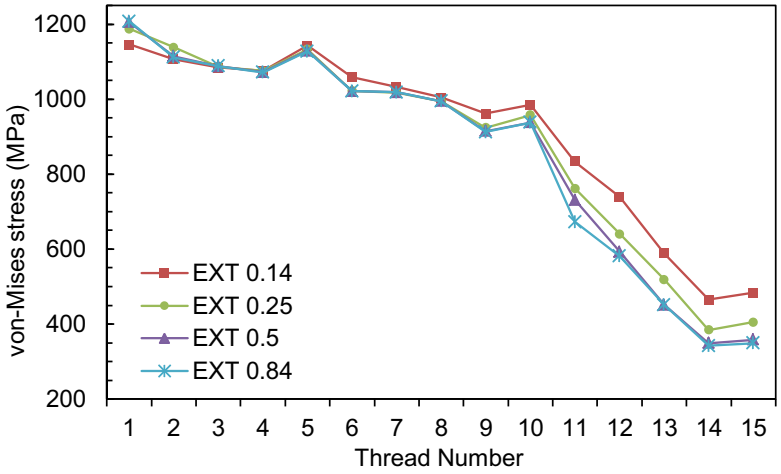

Fig. 10. Maximum stresses per thread (for μ_{TT} 0.84).

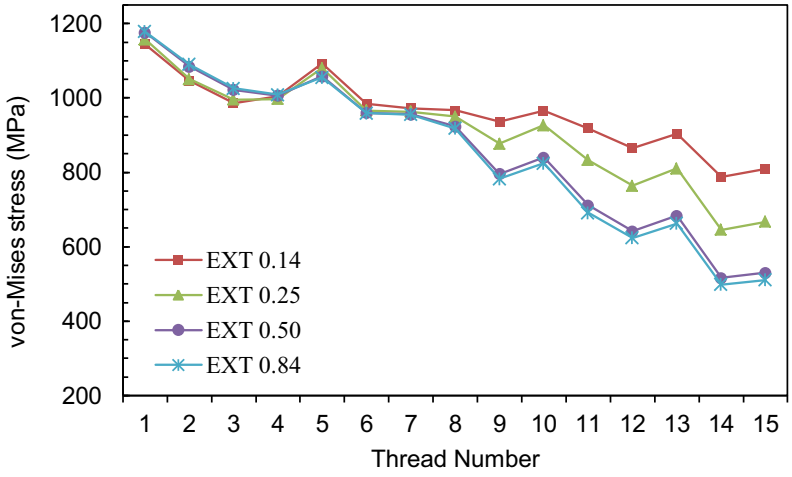

Fig. 11. Maximum stresses per thread (for μ_{TT} 0.14).

Table 7
Average von-Mises stress in the thread (EXT analysis).

μ_{EXT}	0.14	0.25	0.50	0.84
μ_{TT} = 0.84	674	643	630	624
μ_{TT} = 0.14	724	676	636	630
Difference (%)	7.4%	5.1%	1%	1%

Table 8
Analysis of contact pressure between flanges (EXT analysis).

μ_{EXT}	0.14	0.25	0.50	0.84
μ_{TT} = 0.84	113	111	109	108
μ_{TT} = 0.14	113	111	108	107
Difference (%)	0%	0%	1%	1%

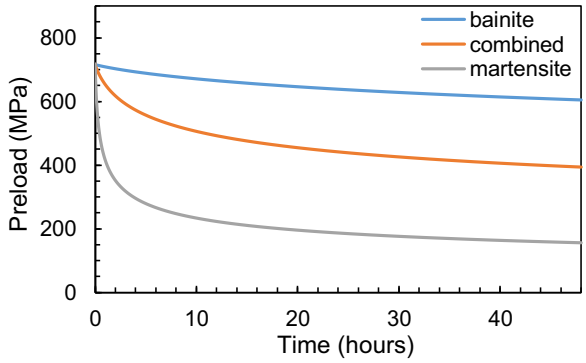

Fig. 12. Preload relaxation after 48-hour period due to creep deformation.

Table 9
Amount of preload relaxation due to creep deformation.

	Stress (MPa) [0h]	Stress (MPa) [48 h]	Reduction
Bainite	717	605	16%
Combined	717	416	42%
Martensite	717	156	78%

lower creep properties could positively reduce creep deformation, as well as minimizing the scatter of preload that could appear if the entirety of the bolt or the flange did not possess the same creep properties.

5.3. Friction effects on low temperature creep

The final set of simulations were performed to examine the effect of friction on bolt relaxation while the material is subjected to time-dependent creep deformation. As it was explained in Section 4, friction has a significant influence on the stress within the bolt and threads. In Fig. 14, the evolution of total preload of the bolt is shown for μ = 0.14 and μ = 0.84, for both EXT and TT contacts. As it was previously mentioned, the lower the friction, the higher the average preload transmitted to the bolt from the tightening process. The time plot of preload shows that creep does not interact much with friction and the difference between the two are constant. Therefore, it can be stated that the friction condition affects the instant of the application of the preload, but does not interfere with short-term low temperature creep.

6. Discussion

6.1. Friction coefficients effects on preload

The simulation results for different combinations of TT and EXT friction coefficients confirm that it is beneficial to operate bolted connections with low friction coefficients. These studies focus on the final stress state of the bolt after applying the specified level of preload. It has been clear that the most influential factor on preload is not μ_{TT} but μ_{EXT}, indicating that lubricating the nut/washer and washer/flange surfaces is beneficial. Well lubricated surfaces offer a higher average stress in the bolt threads. The lower the TT friction, the more noticeable this effect will be. Low μ_{TT} experience a 16% increase in average stress when μ_{EXT} is reduced from 0.84 to 0.14. When a high μ_{TT} is experienced (non-lubricated surface), this increment is only 8%. Although thread friction does have some effect, it is less determinant than EXT friction. A variation on thread friction leads to negligible changes when EXT is 0.84, while a variation of the same magnitude causes up to 7.4% increase when EXT is reduced to 0.14 (lubricated surfaces). It can be concluded that lubricating horizontal surfaces improves the transmission of preload to the bolt, and consequently, the clamping force in the joint.

The results show that increasing EXT friction coefficient reduces contact pressure between the flanges. In this case, however, a change in TT friction coefficient has negligible effect on the contact pressure. This means that a variation of the thread friction does not affect clamping force, as loads can be redistributed in the threads when friction changes. This is not the case for EXT contacts which show an increase of around 5% when the surfaces are lubricated, leading to a low friction coefficient.

Analysing local behaviour in the threads, it seems that depending on the position of the thread, the response to a change in friction is not uniform. There is a descending trend in the thread stresses with the threads closer to the flange experiencing higher stress. From the graphs

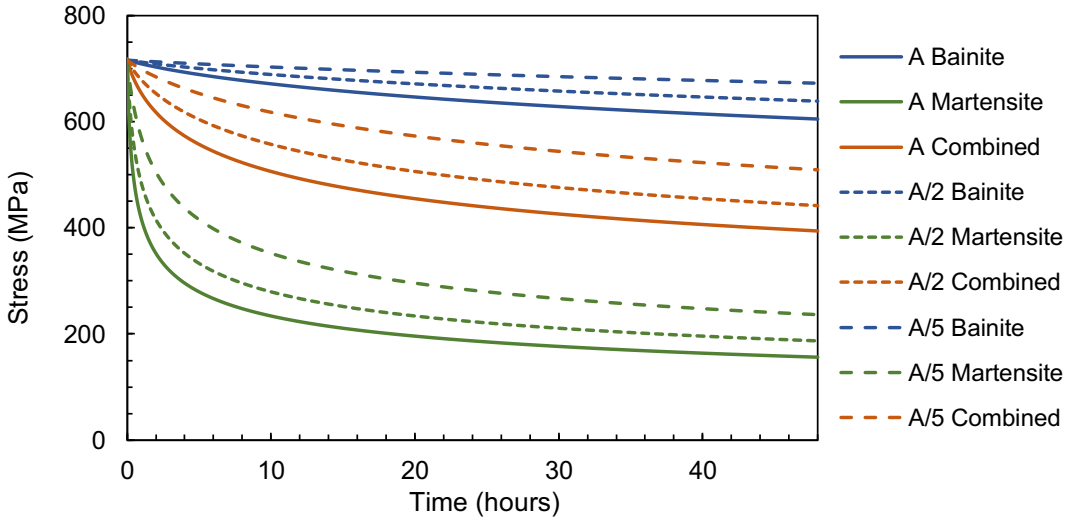

Fig. 13. Sensitivity analysis of preload relaxation to creep power-law multiplier.

Table 10
Sensitivity analysis of preload relaxation to creep power-law multiplier for bainite material.

Factor	Stress (MPa) [0h]	Stress (MPa) [48 h]	Reduction
1	717	605	15.7%
2	717	638	11.0%
5	717	672	6.3%

Table 11
Sensitivity analysis of preload relaxation to creep power-law multiplier combined material.

Factor	Stress (MPa) [0h]	Stress (MPa) [48 h]	Reduction
1	717	416	41.9%
2	717	441	38.4%
5	717	509	29.0%

Table 12
Sensitivity analysis of preload relaxation to creep power-law multiplier for martensite materal.

Factor	Stress (MPa) [0h]	Stress (MPa) [48 h]	Reduction
1	717	156	78.2%
2	717	187	73.9%
5	717	236	67.1%

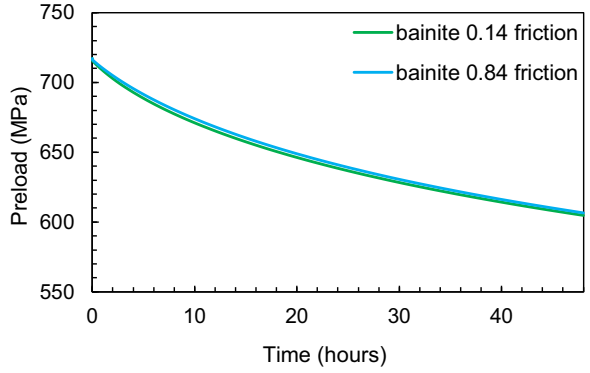

Fig. 14. Friction effects on creep deformation.

shown in Sections 4.1 and 4.2, both TT and EXT friction coefficients affect the stress distribution along the threads. Low friction coefficient lowers the contact point stresses for the first few threads. Given the nature of bolted connections, these stresses will diminish the further they are from the flange. High friction coefficients make this transition abrupt, while on the other hand, better-lubricated contacts (lower friction coefficient) offer a smoother transition. This is interesting as it means low friction contacts contribute to a more efficient work distribution over the thread. It is also important to note that higher local stresses in the initial threads will increase the likelihood of plastic deformation when there are higher levels of friction on all surfaces.

In summary, the combination of all of the results in this section show that the best results is achieved when both TT and EXT surfaces are lubricated and therefore have a low friction coefficient. When this is the case, the maximum stress in the threads are lower, the average stress across the threads are higher and the contact pressure between the flanges is improved.

6.2. Room temperature creep effects on preload

The results presented for the creep simulation were based on approximated material properties from three different high strength steels, however none of them have identical properties to 10.9 grade steel. The results are presented in order to give the reader an idea of the phenomenon being analysed. Therefore, these results should not be considered from a quantitative point of view, as realistic levels of creep experienced by bolts could differ. The present results can however serve as a reference regarding trends and orders of magnitude for room temperature creep in high strength steel bolts.

The first significant conclusion from the creep simulations is that creep can happen in bolted connections at room temperature. Although the creep properties lead to lower $\dot{\varepsilon}_{cr}$ than high temperatures condition, the dependency of $\dot{\varepsilon}_{cr}$ to stress levels make these type of connections susceptible to creep at stresses close to σ_Y. Bolted connections are designed to maintain a minimum preload of around 70% of total σ_Y in the shank, but stresses can reach higher values in some regions with stress concentrators such as the thread of both the bolt and the nut. Bolts are often tightened to preloads closer to σ_Y of the bolt to account for preload relaxation.

As a result, increasing the applied stress in the bolt closer to its σ_Y value (in the present study at around 90%) would increase the stresses in the main part of the bolt as well as the threads, leading to higher creep deformation and greater preload relaxation. It is essential to understand how the creep properties of the material affect the creep

process itself. It is visible from the result that higher σ_Y materials have higher creep resistance with less relaxation encountered.

Using higher strength materials and working closer to 70% of σ_Y could help reducing creep induced relaxation without compromising the required clamping force. If plastic deformation was still required in the nut to ensure the proper tightening of the bolt, different materials could be used for the bolt and nut, provided that they do not have a tendency to chemically interact. Instead of changing the material or altering the load applied at the tightening process, it might be to better to alter the creep properties by other means, such as surface hardening or using shot peening or rolling techniques.

7. Conclusions

Preload relaxation in flange bolted connections is a major concern in offshore wind industry. From the moment the bolt is tightened, a portion of the preload is lost. There are several parameters that govern the relaxation. In this work, two short-term effects including low temperature creep and friction coefficient are investigated using finite element simulations. Friction is shown to have a direct relation with the total preload transmitted, while the results suggest that lower friction improves the transformation of preload into the bolt. Lower levels of friction also contribute to better distribution of the load along the threads, reducing the risk of plasticity in the threads near the washer by allowing subsequent threads to share the load. Although creep is usually neglected for room temperature, the results show that when the applied load is large enough, this assumption is not accurate. Further experiments are required to justify the room temperature creep behaviour for the cases when stresses are close to yield. From the results of the present study, it seems that having materials with yield stresses higher than the working values for the bolt would reduce creep significantly.

CRediT authorship contribution statement

Jarryd Braithwaite: Methodology, Formal analysis, Writing - original draft, Writing - review & editing. **Iñigo Gómez Goenaga:** Formal analysis, Writing - original draft. **Behrooz Tafazzolimoghaddam:** Formal analysis, Writing - original draft. **Ali Mehmanparast:** Conceptualization, Supervision, Writing - review & editing.

Declaration of Competing Interest

None

Supplementary materials

Supplementary material associated with this article can be found, in the online version, at doi:10.1016/j.apor.2020.102225.

References

[1] I. Pineda, The European offshore wind industry, Wind Europe (Key trends and statistics 2016) (2017) 23.

[2] N. Tziavos, H. Hemida, N. Metje, C. Baniotopoulos, Grouted connections on offshore wind turbines: a review, Proc. Inst. Civil Eng. Eng. Comput. Mech. 169 (4) (2016) 183–195.

[3] P. Dallyn, A. El-Hamalawi, A. Palmeri, R. Knight, Experimental testing of grouted connections for offshore substructures: a critical review, Structures 3 (2015) 90–107 Elsevier.

[4] I. Lotsberg, A. Serednicki, O. R, H. Bertnes, A. Lervik, Capacity of cylindrical shaped grouted connections with shear keys in offshore structures, Struct. Eng. 91 (2013) 42–48.

[5] M. Schwedler, S. Dörfeldt, F. Lüddecke, M. Seidel, M. Thiele, Einflussfaktoren auf die Vorspannkraft von Schrauben mit Durchmessern bis M72 in Ringflanschverbindungen, Stahlbau 87 (2) (2018) 149–161.

[6] K.-H. Kloos, Influence of the surface state and the sample size regarding the fatigue strength, VDI-Berichte 268 (1976) 63–76.

[7] S.S. Kadam, S.G. Joshi, Nominal diameter, clamp length and thread pitch analysis for bolt preload augmentation, IJMET 4 (2) (2013) 141–151.

[8] J. Braithwaite, A. Mehmanparast, Analysis of tightening sequence effects of preload behaviour of offshore wind turbine M72 bolted connections, Energies 12 (23) (2019) 4406, , https://doi.org/10.3390/en12234406.

[9] A. Iliopoulos, D. Van Hemelrijck, J. Vlassenbroeck, D.G. Aggelis, Assessment of grouted samples from monopile wind turbine foundations using combined non-destructive techniques, Constr. Build. Mater. 122 (2016) 855–862.

[10] I. Industriales, “Retos en la fabricación y cadena de suministro de aerogeneradores offshore,” 2016. [Online].

[11] G. Kulak, J. Fisher, J. Struik, Guide to Design Criteria for Bolted and Riveted Joints, second ed., American Institute of Steel Construction, Inc., 1988.

[12] M. Kassner, M. Pérez-Prado, Chapter one: introduction, Fundamentals of Creep in Metals and Alloys, Elsevier Science Ltd, 2004, pp. 3–9.

[13] C. Liu, P. Liu, Z. Zhao, D. Northwood, Room temperature creep of a high strength steel, Mater. Des. 22 (4) (2001) 325–328.

[14] J.H. Bickford, Introduction to the Design and Behavior of Bolted Joints: Non-Gasketed Joints, fourth ed., CRC Press, 2007, p. 564.

[15] A. Jacob, A. Mehmanparast, R. D'Urzo, J. Kelleher, Experimental and Numerical Investigation of Residual Stress Effects on Fatigue Crack Growth Behaviour of S355 Steel Weldments, Elsevier, 2019.

[16] Abaqus Inc., “20.2.4 rate-dependent plasticity: creep and swelling products: Abaqus/standard,” 2018. [Online].

[17] T. Anderson, Fracture Mechanics: Fundamentals and Applications, CRC press, 2017.

[18] B. Alfredsson, I. Arregui, J. Lai, Low temperature creep in a high strength roller bearing steel, Mech. Mater. 100 (2016) 109–125 no. ISSN 0167-6636.

[19] International Organization for Standardization, ISO 4032:2012(En): Hexagon regular nuts (style 1) - Product grades A and B, ISO, Geneva, 2012.

[20] D.S. Simulia, Abaqus 6.13 Documentation III Dassault Systemes, 2018.

[21] A. Mehmanparast, C. Davies, G. Webster, K. Nikbin, Creep crack growth rate prediction in 316H steel using stress dependent creep ductility, Mater. High Temp. 31 (1) (2014) 84–94, https://doi.org/10.1179/0960340913Z.00000000011.

[22] R. Shoberg, Engineering Fundamentals of Threaded Fastener Design and Analysis, PCB Load & Torque, Inc., 2000 [Online]. Available: http://www.hexagon.de/rs/engineering%20fundamentals.pdf [Accessed 2018].

[23] P. Andersson, L. Kilpi, K. Holmberg, A. Vaajoki, V. Oksanen, Static friction measurements on steel against uncoated and coated cast iron, Tribologia 34 (1–2) (2016) 5–40.

[24] BVG Associates, Unleashing Europe's Offshore Wind Potentials: a New Resource Assessment, Wind Europe, 2017.

[25] ORE Catapult, Cost Reduction Monitoring Framework 2016 - Summary Report to the Offshore Wind Programme Board, ORE Catapult, 2017.

[26] A Mehmanparast, F Brennan, I Tavares, Fatigue crack growth rates for offshore wind monopile weldments in air and seawater: SLIC inter-laboratory test results, Materials & Design 114 (2017) 494–504, https://doi.org/10.1016/j.matdes.2016.10.070.

[27] A Mehmanparast, J Taylor, F Brennan, I Tavares, Experimental investigation of mechanical and fracture properties of offshore wind monopile weldments: SLIC interlaboratory test results, Fatigue & Fracture of Engineering Materials & Structures 41 (12) (2018).

[28] V Igwemezie, A Mehmanparast, Waveform and frequency effects on corrosion-fatigue crack growth behaviour in modern marine steels, Int. J. Fatigue 134 (2020), https://doi.org/10.1016/j.ijfatigue.2020.105484.

[29] R Redondo, A Mehmanparast, Numerical analysis of stress distribution in offshore wind turbine M72 bolted connections, Metals 10 (5) (2020) 689, https://doi.org/10.3390/met10050689.

[30] V Igwemezie, A Mehmanparast, A Kolios, Current trend in offshore wind energy sector and material requirements for fatigue resistance improvement in large wind turbine support structures–A review, Renewable and Sustainable Energy Reviews 101 (2019) 181–196.

[31] A Mehmanparast, Prediction of creep crack growth behaviour in 316H stainless steel for a range of specimen geometries, Int. J. Pres. Ves. Pip. 120 (2014) 55–65, https://doi.org/10.1016/j.ijpvp.2014.05.006.